Vol 14 No 12, December 2005
1009-1963/2005/14(12)/2552-08
Chinese Physics
© 2005 Chin. Phys. Soc.
and IOP Publishing Ltd

Topology of toroidal helical fields in non-circular cross-sectional tokamaks*

Zha Xue-Jun(查学军)[a)b)†], Zhu Si-Zheng(朱思铮)[b)],
Yu Qing-Quan(虞清泉)[b)], and Wang Yan(王 燕)[c)]

[a)] *State Key Laboratory of High Field Laser Physics, Shanghai Institute of Optics and Fine Mechanics, Chinese Academy of Sciences, Shanghai 201800, China*

[b)] *Institute of Plasma Physics, Chinese Academy of Sciences, Hefei 230031, China*

[c)] *Department of Physics, Shanghai University, Shanghai 200436, China*

(Received 25 January 2005; revised manuscript received 26 May 2005)

The ordinary differential magnetic field line equations are solved numerically; the tokamak magnetic structure is studied on Hefei Tokamak-7 Upgrade (HT-7U) when the equilibrium field with a monotonic q-profile is perturbed by a helical magnetic field. We find that a single mode (m, n) helical perturbation can cause the formation of islands on rational surfaces with $q = m/n$ and $q = (m \pm 1, \pm 2, \pm 3, \ldots)/n$ due to the toroidicity and plasma shape (i.e. elongation and triangularity), while there are many undestroyed magnetic surfaces called Kolmogorov–Arnold–Moser (KAM) barriers on irrational surfaces. The islands on the same rational surface do not have the same size. When the ratio between the perturbing magnetic field $\tilde{B}_r(r)$ and the toroidal magnetic field amplitude $B_{\phi 0}$ is large enough, the magnetic island chains on different rational surfaces will overlap and chaotic orbits appear in the overlapping area, and the magnetic field becomes stochastic. It is remarkable that the stochastic layer appears first in the plasma edge region.

Keywords: plasma equilibrium, magnetic island, stochasticity
PACC: 5255, 0545

1. Introduction

In a toroidal fusion device, confinement properties are closely linked to magnetic topology. A helical perturbation on rational surfaces can cause the formation of island or magnetic ergodic regions, which can deteriorate the confinement of tokamak plasmas in some cases. Normally the transports of energy and particles observed in tokamak experiments greatly exceed the predictions of collisional transport theory. Generally, there are two types of turbulent fluctuations which result in anomalous transports.[1−4] One is drift wave turbulence, corresponding to the stochasticity of particle orbits arising from a perturbing electric field, and the other is magnetic turbulence, corresponding to the stochasticity of magnetic field configuration to some degree originating from a perturbing magnetic field. In recent years, the topology of toroidal magnetic field has aroused the interest of all.[1−12] It is very useful to know both the magnetic topology of tokamak plasmas perturbed by a helical magnetic field and the structure of stochastic layer in the plasma edge region, which is closely related to the improving of plasma confinement. Moreover, the boundary of a diverted tokamak is more sensitive to the loss of magnetic flux to the wall by stochastic transport due to resonant radial field perturbations than the boundary of a non-diverted tokamak. Successful routine tokamak operation in high confinement regimes with current in the external magnetohydrodynamic control coils that are predicted to cause stochastic layers of up to 25% of the poloidal magnetic flux, suggests that either the plasma heals the stochastic region (e.g. through plasma rotation) or the stochastic layer is compatible with edge (H-mode) transport barriers.[12]

2. Theoretical model

In this paper, the differential field line equations in the quasi-cylindrical coordinate system are solved

*Project supported by the National Natural Science Foundation of China (Grant Nos 10405030 and 10135020).
†E-mail: xjzha@siom.ac.cn

using a numerical method, and the topology of the whole magnetic fields in the superconducting tokamak HT-7U[13] (Hefei Tokamak-7 Upgrade) is obtained.

For a magnetically confined plasma such as tokamak, its local thermodynamic equilibrium state is maintained by a strong magnetic field:

$$\nabla p = \boldsymbol{j} \times \boldsymbol{B}. \tag{1}$$

This constraint means that the magnetic field line must lie on a constant pressure surface consistent with the scalar pressure equilibrium. So all of the magnetic surfaces have to be perfectly nested into tori, and all of the field lines that lie on the same surface satisfy an identical rotational transform. If the rotational transform is rational, the field lines spiral around the torus and are closed by themselves. If the rotational transform is irrational, the field line covers the torus ergodically. Whenever a perturbation is present, the topology of the magnetic field will be strongly modified. There appear island chains, together with undestroyed (but deformed) magnetic surfaces called Kolmogorov–Arnold–Moser (KAM) barriers. When the perturbations are large enough, there exist chaotic orbits throughout plasma regions between the island chains on different rational surfaces. In tokamaks, this incompletely chaotic structure is generic, its understanding is a prerequisite for any practical study of transport on such devices. A perturbation can come from external or internal factors. External factors include the error fields caused by technical imperfections in the external toroidal and poloidal coils and ergodization of the edge plasma through deliberate external field perturbations by saddle coils, etc. Internal factors include the magnetic perturbations caused by instabilities and plasma wave. A Poincaré plot is constructed by following a field line numerically for many toroidal laps. The points of intersection of the field lines are plotted in a constant toroidal angle plane and construct a magnetic structure of tokamak. The method is borrowed from classical Hamiltonian mechanics. Indeed, the problem of plotting magnetic field lines is a one-dimensional, time-dependent, Hamiltonian problem. The Poincaré plot is also applied to other fields.[14]

A quasi-cylindrical coordinate is applied in Fig.1. R_Z is the coordinate of magnetic axis; r, θ, φ is a set of coordinates of a so-called toroidal-polar coordinate system, φ a toroidal angle, and θ a similar poloidal angle. The coordinate system is orthogonal apparently and satisfies $\mathrm{d}\boldsymbol{l} \times \boldsymbol{B} = 0$, where $\mathrm{d}\boldsymbol{l}$ is a differential vector tangent to the field line.

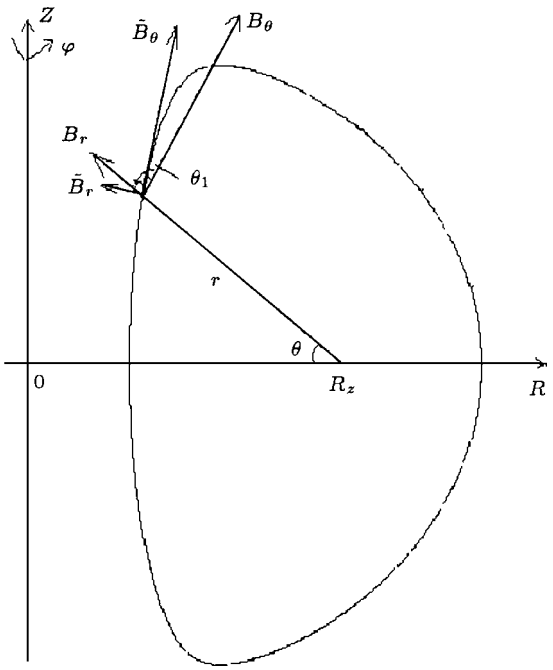


Fig.1. The toroidal–polar coordinate r, θ, φ system, R_Z is the magnetic axis site.

In the coordinate system in Fig.1, the magnetic field line equations become

$$\frac{1}{R}\frac{\mathrm{d}r}{\mathrm{d}\phi} = \frac{B_r}{B_\phi}, \quad \frac{r}{R}\frac{\mathrm{d}\theta}{\mathrm{d}\phi} = \frac{B_\theta}{B_\phi}. \tag{2}$$

An arbitrary magnetic field $\boldsymbol{B}(\boldsymbol{x})$ which does not satisfy Eq.(1) can be still written in the following form in magnetic coordinates ψ, θ, ϕ, ψ_{p}:

$$\boldsymbol{B} = \nabla \Psi \times \nabla\theta + \nabla\phi \times \nabla \Psi_{\mathrm{p}}, \tag{3}$$

therefore, the equations of magnetic field lines become

$$\frac{\mathrm{d}\,\Psi}{\mathrm{d}\phi} = -\frac{\partial\, \Psi_{\mathrm{p}}}{\partial\theta}, \quad \frac{\mathrm{d}\theta}{\mathrm{d}\phi} = +\frac{\partial\, \Psi_{\mathrm{p}}}{\partial\, \Psi}. \tag{4}$$

If there is a field nearby good surfaces one can choose such a $\Psi_{\mathrm{p}}(\Psi, \theta, \phi)$ that

$$\Psi_{\mathrm{p}}(\Psi, \theta, \phi) = \Psi_{\mathrm{p}}(\Psi) + \widehat{\Psi}(\Psi, \vartheta, \phi),$$

with

$$\left|\widehat{\Psi}\right| << |\Psi_{\mathrm{p}}|. \tag{5}$$

This is a standard action (Ψ)-, angle (θ)-, and "time" (ϕ)-dependent Hamiltonian form.[10] The Hamiltonian system, Eqs.(4), (5), is near-integrable and satisfies the KAM theorem. The Hamiltonian form is convenient not only for studying the structure of the magnetic field but also for evaluating the particle drift motion.

In this paper, we use a fourth-order Runge–Kutta method[15] with adaptive stepsize control to solve the differential field line equations. A good ODE integrator should exert some adaptive control over its own progress, making frequent changes in its stepsize. Usually the purpose of this adaptive stepsize control is to achieve some predetermined accuracy in the solution with minimum computational effort. The resulting gains in efficiency are not mere tens percent or a factor of two; they can sometimes be a factor of ten, or a hundred, or more. Using the fourth-order Runge-Kutta method with adaptive stepsize control we calculate some comparatively complicated ordinary differential equations that have also their analytic solutions, and compare the numerical results with the analytic solutions. It shows that the accuracy of the applied Runge–Kutta method is sufficient. By using a numerical technique, we obtain the topology of toroidal helical fields in a non-circular cross-sectional tokamak equilibrium that is subject to a helical magnetic perturbation. From Eq.(2), we can obtain

$$\frac{\mathrm{d}r}{\mathrm{d}\phi} = \frac{R(B_{r0}+B_{r1})}{B_\phi} = \frac{(R_z - r\cos\theta)^2(B_{r0}+B_{r1})}{R_z B_{\phi 0}}, \tag{6}$$

$$\begin{aligned}\frac{\mathrm{d}\theta}{\mathrm{d}\phi} =& \frac{R(B_{\theta 0}+B_{\theta 1})}{rB_\phi} \\ =& \frac{(R_z - r\cos\theta)^2(B_{\theta 0}+B_{\theta 1})}{rR_z B_{\phi 0}},\end{aligned} \tag{7}$$

where $\boldsymbol{B}_0$ is an equilibrium field, and $\boldsymbol{B}_1$ is a perturbing field; they satisfy $\nabla\cdot\boldsymbol{B} = \nabla\cdot(\boldsymbol{B}_0+\boldsymbol{B}_1) = \nabla\cdot\boldsymbol{B}_1 = 0$. Because $\tilde{B}_\varphi$, the toroidal component of $\boldsymbol{B}_1$, satisfies $\left|\tilde{B}_\varphi\right| << |B_{\phi 0}|$, $\boldsymbol{B}_1$ satisfies $\nabla\cdot\boldsymbol{B}_1 = \nabla\cdot(\tilde{B}_r\boldsymbol{e}_r + \tilde{B}_\theta\boldsymbol{e}_\theta) = 0$ with the toroidal magnetic field perturbation ignored, namely

$$\tilde{B}_r + r\frac{\partial\tilde{B}_r}{\partial r} + \frac{\partial\tilde{B}_\theta}{\partial\theta} = 0, \tag{8}$$

which corresponds to tearing mode perturbations. Here, Eq.(8) is dealt with in the cylindrical model approach. In some other papers, $\tilde{B}_r$ is calculated only with $\tilde{B}_\theta$ ignored, thus it is equivalent to the ignoring of the compressive Alfven wave effect. If radial magnetic field perturbations are assumed to be

$$\tilde{B}_r(r,\theta,\phi) = \sum_{m,n=0}^{\infty}\tilde{B}_r(r)\mathrm{e}^{\mathrm{i}(m\theta-n\phi)}, \tag{9}$$

and a simplified model for magnetic perturbation is considered which does not take into account its radial dependence,[16] we can think $\tilde{B}_r(r)$ to be independent of coordinate r and the amplitude of $\tilde{B}_r(r)$ to be the same constant on different surfaces. According to the assumption, it is easy to separate $\tilde{B}_r$and $\tilde{B}_\theta$in Eq.(8) for the convenience of numerical calculation.

Substituting Eq.(9) into Eq.(8) leads to

$$\tilde{B}_\theta(r,\theta,\phi) = \sum_{m,n=0}^{\infty}\frac{1}{m}\tilde{B}_r(r)\mathrm{e}^{\mathrm{i}(m\theta-n\phi)},$$

where $\tilde{B}_r(r,\theta,\phi)$ and $\tilde{B}_\theta(r,\theta,\phi)$ are vertical and tangential magnetic perturbations in magnetic surfaces respectively, distinguished from B_{r1} and $B_{\theta 1}$ in Eqs.(6) and (7). The geometrical relations between them are $B_{\theta 1} = \tilde{B}_\theta\cos\theta 1 - \tilde{B}_r\sin\theta 1$, and $B_{r1} = \tilde{B}_\theta\sin\theta 1 + \tilde{B}_r\cos\theta 1$ in Fig.1, where the poloidal angle $\theta 1$ is determined by $\theta 1 = a\tan(B_{r0}/B_{\theta 0})$, and the equilibrium field $\boldsymbol{B}_0(B_{r0}, B_{\theta 0})$ is from an axisymmetric Grad–Shafranov plasma equilibrium solver using the EQ code.[17,18] Thus, substituting these variables into Eqs.(6), (7), the magnetic field Eqs.(6), (7) are solved numerically.

It should be noted that the assumption in which $\tilde{B}_r(r)$ is independent of coordinate r is reasonable in the paper. This is because our main interest is focused on the topology of tokamaks with weak magnetic perturbations. All of irrational surfaces are not undestroyed when the perturbed magnetic field is very weak ($\tilde{B}_r(r)/B_{\phi 0} \le 10^{-4}$). Namely the topology on irrational surfaces is independent of the perturbation, so we simply care for the topology on rational surfaces. In lots of numerical results, we find the changes of the results to be quite weak in the topology on a rational surface between those perturbations depending and not depending on their forms with a weak perturbing field. Moreover, for those magnetic perturbations induced by all kinds of instabilities from inner plasma, the perturbed form is still an open question so far; for those magnetic perturbations produced by external factors, e.g. the resonant magnetic perturbation coils, the perturbing magnetic field can be accurately calculated with Biot–Savart law and transformed into a Fourier form in toroidal and poloidal directions, then forms of the different perturbation modes (m, n) can be known, so it is easy to consider the topology of the external perturbing field form in the calculation of the magnetic field.

3. Numerical results

The field line equations (6), (7) are numerically integrated and mapped. Each point is the intersection of a magnetic line with a transversal plane af-

ter one toroidal lap. Here, the $\boldsymbol{B}_0(B_{r0}, B_{\theta 0})$ at any point on the equilibrium surface is obtained with a fitting two-dimensional bicubic spline interpolation method which has a high accuracy in calculation. The maps are showed with a developed numerical tool TFEC using typical values of HT-7U: plasma current $I_{\rm p}$=1MA, major radius R_0 =1.92m, small radius a=0.47m, magnetic axis R_z=1.98m, and toroidal magnetic field $B_{\phi 0}$=3.5T.

Figure 2(a) shows the q-profile computed by the EQ code. In this case, q varies between 1.10 at the axis and 6.45 on the plasma edge. Figure 2(b) is the map without perturbations, in which each magnetic surface plot is produced with a starting point, and the field lines on each surface are integrated for 600 toroidal laps. From Fig.2(b), the magnetic flux surfaces are perfectly nested into tori, showing the accuracy in calculation to be high enough by using the Runge–Kutta method. With perturbations, for those particular perturbing modes on rational surfaces, $q = m/n$ (4/2, 6/2, 8/2, 6/3, $\cdots$) which is of fractional reduction, we find that the corresponding surface plot is produced with n starting points at least in numerical calculations; for the near separatrix region, it is very easy for field lines to diffuse out of the separatrix surface and become open due to magnetic perturbations, so we have to deal with the small structures in the stochastic edge region carefully. The plot of each magnetic surface in the near separatrix region is obtained with lots of starting points which come from the magnetic surface in equilibrium and each starting point traces no more than 10 toroidal laps; besides the above case, each magnetic surface is produced with a starting point for all of the plots in the whole plasma region, and field lines on each surface are integrated for 600 toroidal laps.

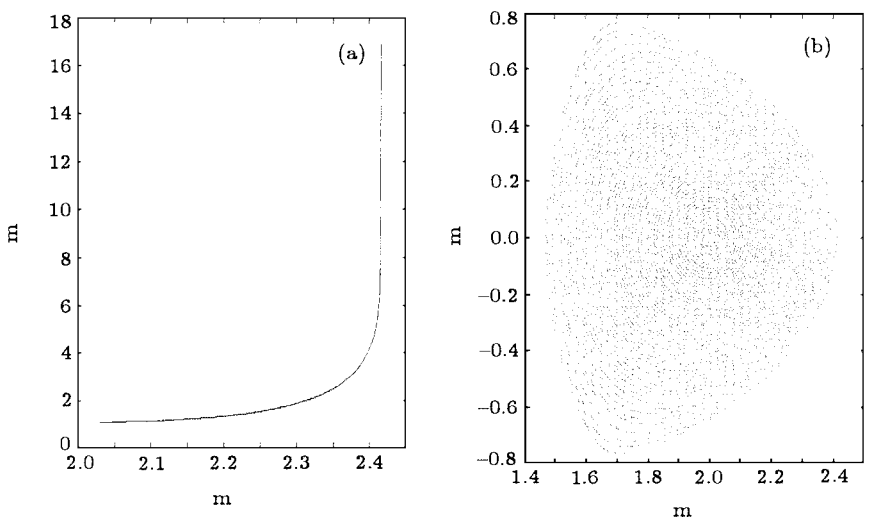


Fig.2. (a) The safety factor q profile. (b) The numerical map of magnetic field structure in HT-7U equilibrium without magnetic perturbation.

Figures 3–7 show the magnetic structures in a constant toroidal angle plane for the HT-7U tokamak under different conditions. In Fig.3(a), a single m/n=2/1 helical perturbation is introduced to all magnetic surfaces, which causes the islands on rational surfaces with q=2/1, 3/1, 4/1 and 5/1. A single m/n=3/1 perturbation can also cause the islands on the same rational surfaces as those in the m/n=2/1 perturbation case (Fig.3(b)). As for a single m/n=3/2 perturbation, the islands on rational surfaces with q=3/2, 4/2, 5/2, 6/2, 7/2, 8/2, 9/2 and 10/2 are clearly visible in Fig.3(c). In order to show the phenomenon more clearly, Fig.4 only gives the magnetic structures on the corresponding rational surfaces. It means that a single helical perturbation mode (m, n) can cause the formation of islands on the rational surface not only with $q = m/n$ but also with $q = (m \pm 1, 2, 3, \cdots)/n$, i.e. the same toroidal mode number n and different poloidal mode numbers m are coupled as a global structure due to the toroidicity and shaped cross-section. Moreover, the widths of the islands on the same resonant surface are not equal and their locations are of poloidal asymmetry, as can be seen from these figures. Figure 5 shows the magnetic structure with multi-mode magnetic perturbations. The only difference among

Fig.5(a)–(c) is the ratio $\tilde{B}_r(r)/B_{\phi 0}$. Figure 5(a) corresponds to a ratio of 10^{-5}, while 10^{-4} for Fig.5(b) and 5×10^{-4} for Fig.5(c). Because the magnetic perturbation is very weak, the structure of magnetic field in Fig.5(a) is basically undestroyed. But when the magnetic perturbation becomes larger, it can exert a strong influence on plasma edge and a stochastic layer starts on the edge, as shown in Fig.5(b). The figure also displays many magnetic island chains on rational surfaces in the plasma core. On the contrary, the magnetic surfaces on which the safe factor q is irrational are not affected by the perturbing field and are still perfect by nested toroidal surfaces in Figs.3(a)–(c) and Figs.5(a)–(b). The magnetic perturbations increase further in Fig.5(c), the magnetic island chains in the core region, formed by multi-mode perturbations on different rational surfaces, have overlapped. This leads to chaotic orbits and highly stochastic magnetic field there. Since particles following a chaotic field line may experience rapid radial transport, the chaotic structure is one of the reasons that result in anomalous transports.

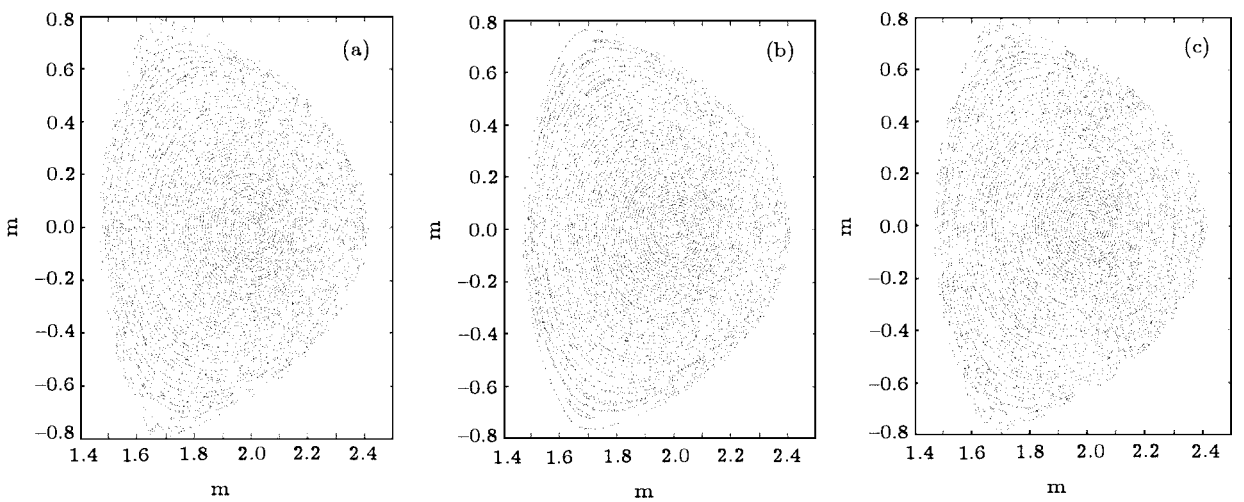


Fig.3. The numerical map of magnetic structure in the whole plasma region with a single mode perturbation, the ratio $(\tilde{B}_r(r)/B_{\phi 0})$ is 10^{-4} in (a)–(c). (a) m/n=2/1. (b) m/n=3/1. (c) m/n=3/2.

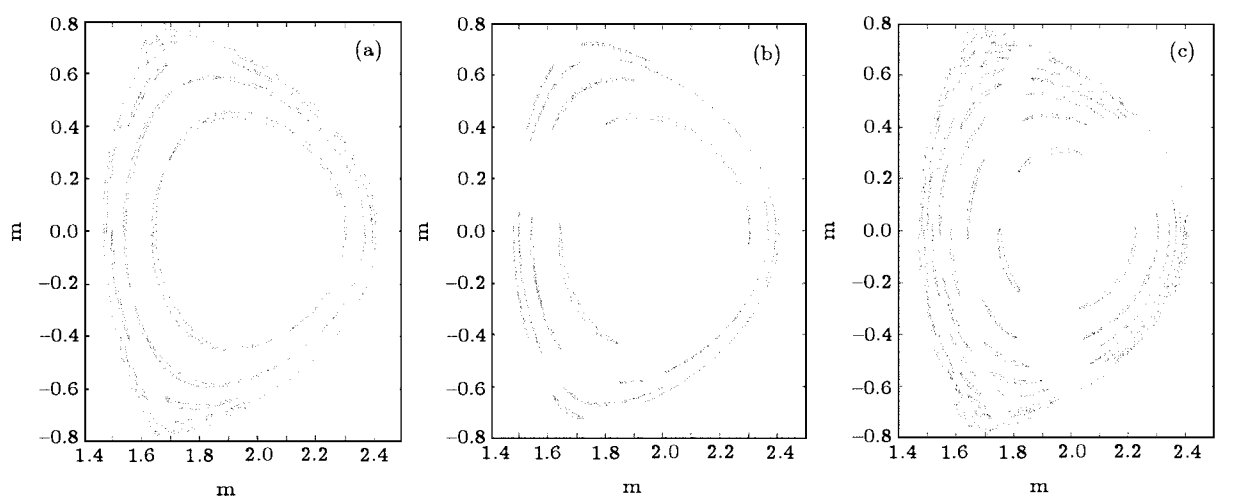


Fig.4. The magnetic islands on rational surfaces with a single mode perturbation, the ratio $(\tilde{B}_r(r)/B_{\phi 0})$ is 10^{-4} in (a), (b), (c). (a) m/n=2/1. (b) m/n=3/1. (c) m/n=3/2.

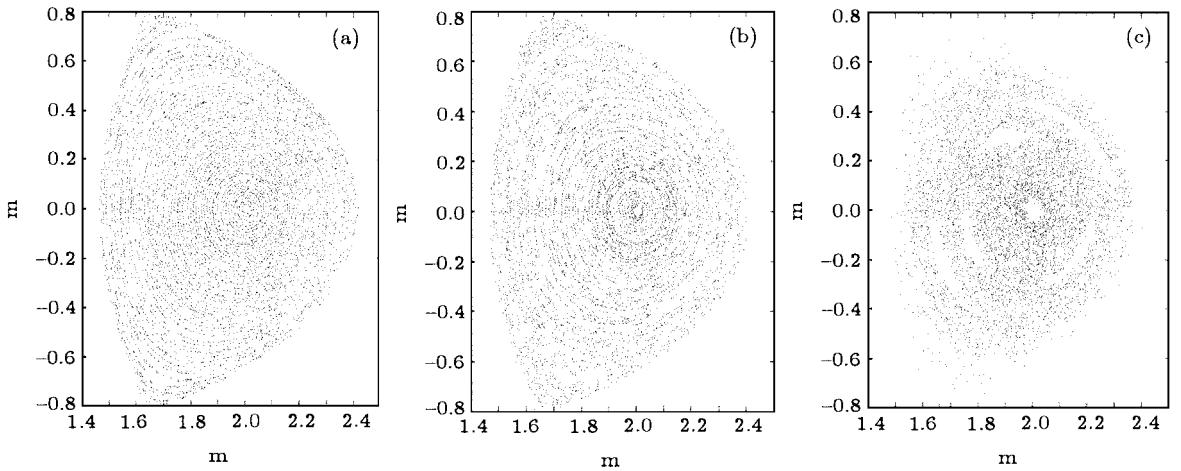


Fig.5. The numerical map of magnetic structure in the whole plasma region in (a), (b) and in the core plasma region in (c) with multi-mode perturbations. (a) The ratio $(\tilde{B}_r(r)/B_{\phi 0})$ is 10^{-5}. (b) The ratio is 10^{-4}. (c) The ratio is 5×10^{-4}.

It is remarkable that the global stochasticity starts in the plasma edge region first. This is because of the magnetic shear being very large in the vicinity of separatrix surface, the interval between those rational surfaces in the edge region is very short and the magnetic islands can overlap easily when the perturbations are large enough. In order to show the point, we present a qualitative analysis of a single mode perturbation in Figs.6(b)–(c) and multi-mode perturbations in Figs.7(a)–(c) respectively. The magnetic structure in the edge region nearby the separatrix surface is given in Figs.6–7. Figure 6(a) shows the separatrix area near X-point with no perturbation, where the magnetic surfaces perfectly consist of nested flux surfaces. When the ratio $(\tilde{B}_r(r)/B_{\phi 0})$ for a single mode m/n=2/1 perturbation ranges from 10^{-4} in Fig.6(b) to 5×10^{-4} in Fig.6(c), the stochastic layer clearly appears in Fig.6(c). Similar features also appear for multi-mode perturbations in Figs.7(a)–(c). Moreover, the stochastic layer formed by multi-modes starts with less perturbations than those in the case of a single mode. That is to say it is easier to form edge stochastic layer for multi-mode perturbations.

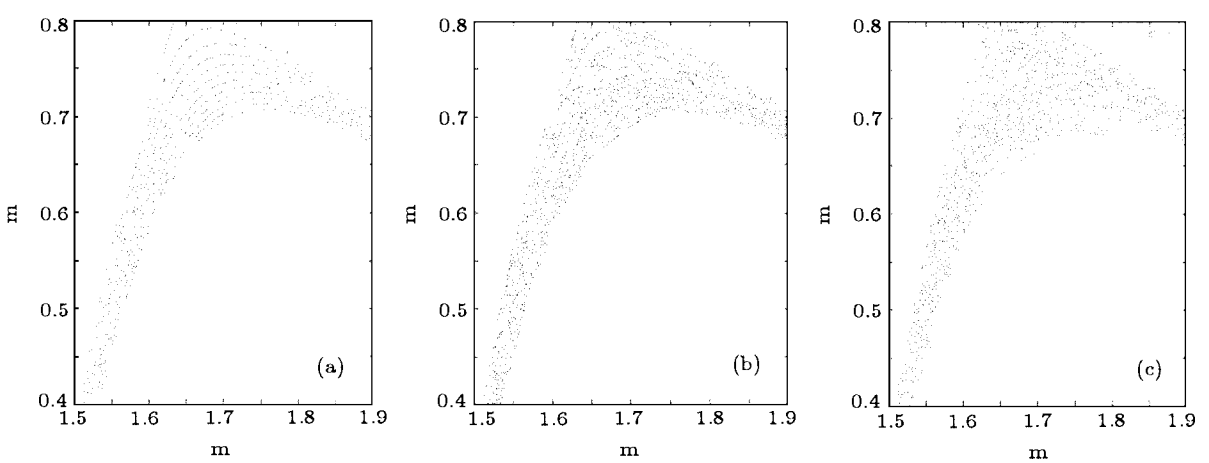


Fig.6. The magnetic structure in edge region near the separatrix surface. (a) no perturbation. (b) A single mode m/n=2/1 with the ratio $(\tilde{B}_r(r)/B_{\phi 0})$ being 10^{-4}. (c) A single mode m/n=2/1, with the ratio being 5×10^{-4}.

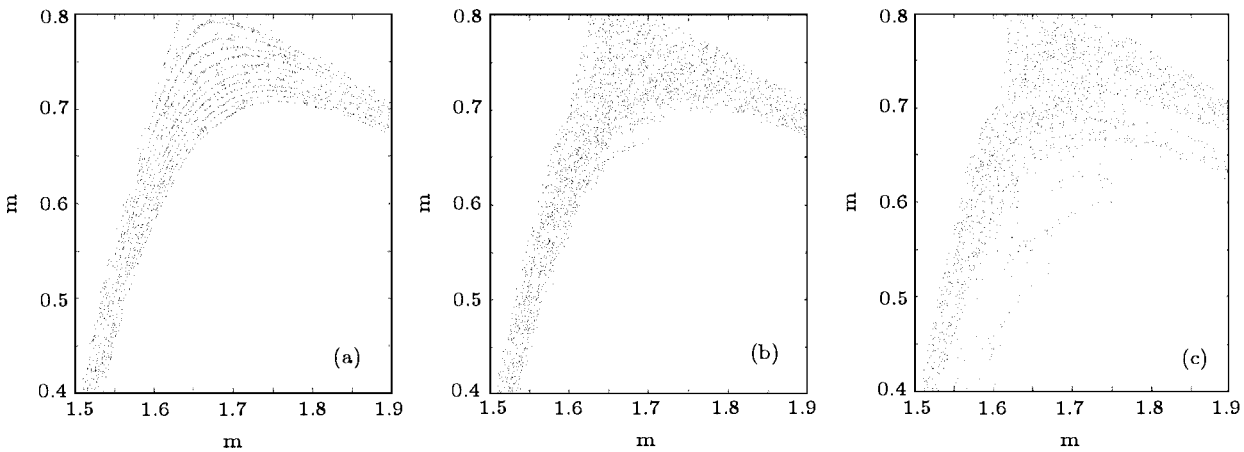


Fig.7. The magnetic structure in the edge region near the separatrix surface with multi-mode perturbations with the ratios $(\tilde{B}_r(r)/B_{\phi 0})$ being 10^{-5} (a), 10^{-4} (b), and 5×10^{-4} (c).

4. Summary

In this paper, only one situation is considered in which there exists a monotonous profile of safety factor (namely twist condition). In a tokamak plasma, the same toroidal mode number n and different poloidal mode numbers m are coupled as a global structure due to the toroidicity, so a single mode (m, n) helical perturbation causes the formation of islands on rational surfaces with $q = m/n$ and $q = (m \pm 1, \pm 2, \pm 3, \cdots)/n$; this extends Monteiro's conclusion[7] that a single perturbing helical mode (m, n) only can cause islands on a rational surface with $q = m/n$ and $q = (m \pm 1/n)$. As a consequence of toroidicity, the poloidal positions of magnetic islands on the same resonant surface do not have any symmetry and the same widths. In all our numerical calculations, when the magnetic field perturbation level is the same, we find that low mode rather than high mode perturbations are easier to affect magnetic surface structure and form islands; this phenomenon has been observed in tokamak experiments. The ratio of $\tilde{B}_r(r)/B_{\phi 0}$ to make magnetic fields stochastic for multi-mode perturbations is less than 10^{-4}, which is lower than that for a single mode perturbation. It is remarkable that stochastic layer appears first in the plasma edge region. Increasing the multi-mode magnetic perturbations further (the ratio for multi-mode perturbations is $\tilde{B}_r(r)/B_{\phi 0} \geq 10^{-4}$ level), the magnetic surfaces in the whole plasma region are destroyed drastically, thereby the KAM theory is inapplicable. This leads to a highly stochastic magnetic field and the plasma being in strongly chaotic state. But there is not evidence that the plasma always remains in a strongly chaotic state: charged particles would not be confined in that case. Thus, the magnetic perturbations are at a modest level at best, and their effect is subtle.

Acknowledgement

The authors are grateful to Professors Yu Guo-Yang and Wang Shao-Jie for their interest and discussion. The authors are also grateful to Professor Wang Ke-Wu for grammatical corrections in the revised paper.

References

[1] Cardozo N L 2002 *Trans. Fusion Sci. Technol.* **41** 163

[2] Bickerton R J 1997 *Plasma Phys. Control. Fusion* **39** 339

[3] Connor J W and Wilson H R 1994 *Plasma Phys. Control. Fusion* **36** 719

[4] Wang W H, Xu Y H, Yu C X, Wen Y Z, Ling B L, Song M and Wan B N 2001 *Acta Phys. Sin.* **50** 1956 (in Chinese)
Wang W H, Yu C X, Wen Y Z, Xu Y H, Ling B L, Gong X Z, Liu B H and Wan B N 2001 *Chin. Phys.* **10** 139

[5] Donne A J H, Van Gorkom J C, Udintsev V S, Domier C W, Kramer-Flecken A, Luhmann N C, Jr, Schuller F C and TEXTOR team 2005 *Phys. Rev. Lett.* **94** 085001

[6] Balescu R, Vlad M and Spineanu F 1998 *Phys. Rev.* E **58** 951

[7] Monteiro L H A, Okano V, Kucinski M Y and Caldas I L

1994 *Phys. Lett.* A **193** 89
[8] Fischer O 2001 *LRP* **693/01** April
[9] Zheng S B 1995 *Acta Phys. Sin.* **44** 715 (in Chinese)
[10] Boozer A H 1983 *Phys. Fluids* **26** 1288
[11] Garcia L, Carreras B A, Lynch V E, Pedrosa M A and Hidalgo C 2001 *Phys. Plasmas* **8** 4111
[12] Evans T E, Moyer R A and Monat P 2002*Phys. Plasmas* **9** 4957
[13] Wan Y X, HT-7 Team and HT-7U Team 2000 *Nucl. Fusion* **40** 1057
[14] Gao Y, Weng J Q, Fang J Q and Luo X S 2001 *Acta Phys. Sin.* **50** 1440 (in Chinese)
Li W and Chen S G 2001 *Acta Phys. Sin.* **50** 1434 (in Chinese)
[15] Press W H, Flannery B P, Teukolsky S A and Vetterling W T 1986 *Numerical Recipes* (Cambridge University Press)
[16] Abdullaev S S, Finken K H, Jakubowski M W, Kasilov S V, Kobayashi M, Reiser D, Reiter D, Runov A M and Wolf R 2003 *Nucl. Fusion* **43** 299
[17] Zha X J, Zhu S Z and Yu Q Q 2002 *Chin. J. of Computational Phys.* **19** 413
[18] Zha X J, Zhu S Z and Yu Q Q 2003 *Acta Phys. Sin.* **52** 1981 (in Chinese)